Photochemistry of Matrix-Isolated and Thin Film Acid Chlorides: Quantum Yields and Product Structures

Brad Rowland,[†] Paul R. Winter,[‡] G. Barney Ellison,[‡] Juliusz G. Radziszewski,[§] and Wayne P. Hess*,[†]

Pacific Northwest National Laboratory, P.O. Box 999, Richland, Washington 99352, Department of Chemistry & Biochemistry, University of Colorado, Boulder, Colorado 80309, and National Renewable Energy Laboratory, 1617 Cole Boulevard, Golden, Colorado 80401

Received: September 17, 1998; In Final Form: November 5, 1998

Ultraviolet photoexcitation of matrix-isolated CH_3COCl, CH_3CH_2COCl, and $CH_3CH_2CH_2CH_2COCl$ produces $HCl{\cdot}CH_2{=}C{=}O$, $HCl{\cdot}CH_3CHC{=}C{=}O$, and $HCl{\cdot}CH_3CH_2CH_2CHC{=}C{=}O$ complexes. We report precursor and matrix dependent reaction quantum yields. Quantum yield values decrease with increasing alkyl chain length due to a reduced number of α H-atoms available for the elimination reaction and steric considerations. We found quantum yields in neat matrixes to be roughly half that in argon or xenon matrixes and assign structures for HCl and ketene complexes in argon and xenon matrixes by comparing IR spectra to ab initio electronic structure calculations. In argon matrixes, the product complex HCl frequency is strongly shifted whereas the ketene remains unshifted with respect to matrix-isolated ketene. In xenon matrixes, HCl·ketene complexes display absorption bands indicative of two distinct structures**.** Differences between HCl·ketene structures in argon and xenon matrixes are attributed to size differences of the matrix lattice.

Introduction

Studying the differences between gas- and condensed-phase photochemistry strengthens our understanding of many-body interactions in reactive processes. The photoreactivity of small molecules can be highly sensitive to phase, and well-known gas-phase reaction mechanisms are often modified in the condensed phase or completely subsumed by other distinct reactive channels. The extension of gas-phase results to heterogeneous surfaces is often done for reactions of relevance to combustion and atmospheric chemistries. An excellent illustration of phase sensitive reactivity is found in the photochemistry of acid chlorides. For example, the ultraviolet (∼250 nm) photoreaction of acetyl chloride in neat and matrix-isolated films produces HCl·ketene ($H_2C{=}C{=}O$) complexes exclusively through an elimination reaction[1,2] while the well-studied gas-phase photodissociation initially produces Cl and acetyl radicals. In the gas-phase reaction, a fraction of initial acetyl radical product may further decompose to methyl radical and CO.[3−6] In this paper, we consider the photoreaction of condensed acid chloride samples by comparison of reaction quantum yields for acetyl (CH_3COCl), propionyl (CH_3CH_2COCl), and valeryl ($CH_3CH_2CH_2CH_2COCl$) chlorides. The relationship of product geometry (in various matrixes) to infrared spectra and quantum yield determinations is discussed.

The gas-phase photoreaction of acetyl chloride involves an initial excitation to the $^1[n, \pi^*(C{=}O)]$ state immediately followed by interconversion to the repulsive $^1[n, \sigma^*(C{-}Cl)]$ state on an excited singlet surface.[4,7,8] The impulsive gas-phase dissociation occurs on a femtosecond time scale.[5] A similar dissociation reaction is observed for the far UV (193 nm) photolysis of condensed acetyl chloride.[2] However, the ∼250 nm photoreaction of condensed acetyl chloride appears to undergo an elimination reaction on the ground electronic surface to produce geminate HCl·ketene complexes.[2] Similar photoreactive mechanisms describe the gas- and condensed-phase reactions of propionyl chloride following 248 nm photoexcitation.[9]

Although the mechanism of condensed-phase photoreaction is described as an elimination process, the detailed reaction path is unknown. We consider two distinct reaction mechanisms; (1) initial distribution of the internal excitation statistically into the vibrational modes of the acid chloride molecule and (2) mode specific distribution of localized excitation channeled more or less directly into the vibrational modes associated with the reaction coordinate. If the time scale of the reaction is sufficiently long, the internal excitation can be redistributed into the intramolecular vibrational modes such that the subsequent reaction should be described by statistical reaction rate (RRKM) theory.[10] A statistically based mechanism should yield the same products as observed in thermally activated unimolecular reactions. For example, chloroethane produces HCl and ethylene in shock-initiated reactions[11] but produces Cl and CH_3CH_2 radicals when irradiated at 193 nm.[12] In a chemical activation study by Srivatsava et al., the addition of an H-atom to CH_2COCl radical produces a chemically activated acetyl chloride molecule that undergoes elimination to form HCl and ketene.[13]

Assuming the initial photoexcitation becomes statistically distributed into the vibrational modes of the S_0 acid chloride, we expect the reaction quantum yields to dramatically decrease as the number of vibrational modes increase throughout the series CH_3COCl, CH_3CH_2COCl, and $CH_3CH_2CH_2CH_2COCl$. The calculated reaction rates favor reaction of acetyl chloride over reaction of propionyl chloride by a factor of 200, and over valeryl chloride by a factor greater than one million.[14] We would therefore expect the condensed-phase reaction quantum yields

* Corresponding author. E-mail: wayne.hess@pnl.gov.
[†] Pacific Northwest National Laboratory.
[‡] University of Colorado.
[§] National Renewable Energy Laboratory.

10.1021/jp9837481 CCC: $18.00
Published on Web 01/29/1999

to be greatly determined by alkyl chain length for a statistical reaction mechanism.

However, if the initial photoexcitation (localized along the C═O bond) leads directly to motion toward the reaction transition-state structure, then the relative condensed-phase quantum yields may depend on the number of available α-H-atoms and steric factors. If mode specificity occurs within acid chlorides, the total number of vibrational modes will have little effect on the reaction quantum yields. Mode specific distribution of photoexcitation energy into motion along the reaction coordinate is observed in the photolysis of formaldehyde.[10] There, energy is preferentially distributed into the antisymmetric C−H stretch and the H−C−H deformation, modes leading to the transition state geometry required to form H_2 and CO.

The condensed-phase quantum yields may also be affected by energy loss to the matrix, such that reactions occurring in neat matrixes, where vibrational energy transfer is efficient, will have lower quantum yields than in matrixes, such as argon, where energy transfer is less efficient. The many vibrational modes within the neat matrix promote efficient energy transfer. In the gas phase, Miller and Barker[15] have shown that the self-relaxation of vibrationally excited pyrazine is 21 times more efficient than relaxation by collisions with argon.

We use Fourier transform infrared (FTIR) absorption spectroscopy to study the photodynamics of thin films of acid chlorides irradiated at 248 and 266 nm and to determine the reaction quantum yields. Considerable attention is given to measure accurate values for IR and UV molar absorptivities that are used to determine quantum yields. Changes in absorption band centers and intensities due to intermolecular interaction with surrounding molecules can significantly alter molar absorptivities from gas-phase values.[16] Significant changes in IR band center frequencies and integrated intensities are observed for hydrogen-bonded molecules such as H_2O and HCl. For example, the IR spectrum of HCl adsorbed onto a LiF(100) surface is red shifted ∼300 cm^{-1} with respect to the gas-phase value, and the IR intensity is increased by more than 1 order of magnitude.[16] Although condensed-phase IR spectra generally show a red shift of band frequencies, due to shifting of electron density to form intermolecular bonds, the electronic spectra may display a blue shift. Berg et al. observed such a blue shift of the UV absorption bands for ketene adsorbed on the surface of NaCl (100).[17]

While IR frequency band shifts and absorbtivity enhancements of HCl can complicate quantum yield determinations, such effects can be used as a probe of intermolecular bonding in matrix-isolated photoproduct complexes. By using the HCl band shift as a probe, we can assign structures to product complexes in various matrixes. Previously, polarized infrared spectroscopy was used to study the orientation of the HCl·ketene complex in argon matrixes. We argued that the complex structure is roughly "T" shaped with the hydrogen of HCl bonded to the methylenic carbon of ketene (Figure 1). This structure is similar to the transition-state geometry for the elimination reaction calculated by Sumathi and Chandra.[18] Structure **1** also corresponds to the most stable dimer geometry predicted by ab initio calculations.[19] However, another stable hydrogen-bonded dimer geometry exists. This second structural minima involves the hydrogen of HCl bonding to the oxygen of ketene. In this paper, we also describe and assign the structures of HCl·ketene complexes for the 248 and 266 nm photoreaction of acetyl chloride in xenon and argon matrixes.

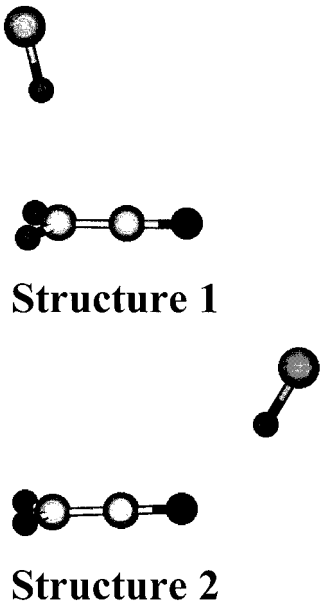

Figure 1. Structures **1** and **2** of the HCl·ketene complexes. IR spectra assigned to both structures **1** and **2** are observed in xenon matrixes. Only IR bands assigned to structure **1** are observed in argon matrixes. Structures are as calculated in ref 19.

Experimental Section

Neat and argon matrix-isolated thin films of acid chlorides are deposited onto KBr and BaF_2 substrates cooled to about 20 K by a closed-cycle helium cryostat. Thin films are vapor deposited through a single nozzle or by back-filling (through a leak valve) our UHV chamber to pressures of roughly 10^{-4} Torr, such that deposits are approximately 2 μm (neat) or 6−9 μm (rare-gas matrixes) thick. For the matrix-isolated samples, a concentration of 300:1 argon to acid chloride is used. All acid chloride samples were obtained from commercial vendors at stated purities of 99% or greater.

Thin film growth is monitored by recording the intensity of the reflected 633 nm helium−neon laser beam that is aligned at a near-normal angle to the deposit. As the sample thickness increases, the intensity of the reflected beam oscillates due to constructive and destructive interference. The thickness d is given by $d = N\lambda/2\eta$, where the number of oscillations, the index of refraction, and the wavelength of the laser are represented by N, η, and λ, respectively.[20] To our knowledge, index of refraction values are not reported for solid acetyl, propionyl, and valeryl chlorides. Therefore, we use the commercially reported liquid values of 1.39 ± 0.01 (CH_3COCl), 1.40 (CH_3CH_2COCl), and 1.42 ($CH_3CH_2CH_2CH_2COCl$) to estimate neat sample thickness.[21] For solid argon, we use the reported index of refraction value of 1.29 ± 0.01.[22]

Matrix-isolated and neat deposits are irradiated at 248 and 266 nm using the emission from an excimer laser and the fourth harmonic of a Nd:YAG laser, respectively. For the 248 nm photoexcitation, samples are irradiated for 1 min using an average pulse energy of 6 mJ at a 10 Hz repetition rate with a 1.1 cm beam diameter. For the photoexcitation at 266 nm, films are irradiated for 5 min using an average pulse energy of 1.5 mJ at a 20 Hz repetition rate with a 1.9 cm beam diameter. Pulse power is measured immediately before the laser beam enters the vacuum chamber. To determine accurate photon fluxes, we account for losses due to reflection (8%) and absorption of the quartz window.

Infrared spectra of condensed samples are collected at a resolution of 2 cm^{-1} before and after irradiation at 248 and 266

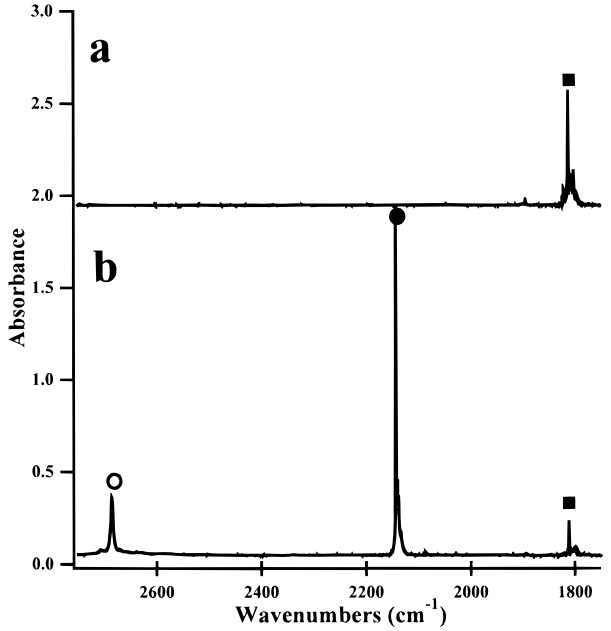

Figure 2. Infrared spectra of acetyl chloride (CH_3COCl) before (a) and after (b) 248 nm irradiation. The C═O stretch band of the acetyl chloride is marked by filled squares. The C═O and HCl stretches of the ketene and HCl are marked by filled and open circles, respectively.

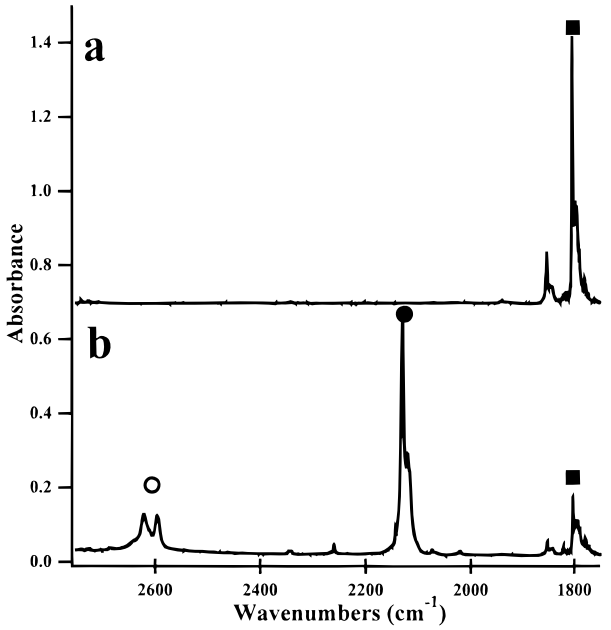

Figure 3. Infrared spectra of propionyl chloride (CH_3CH_2COCl) before (a) and after (b) 248 nm irradiation. The C═O stretch band of the propionyl chloride is marked by filled squares. The C═O and HCl stretches of the methylketene and HCl are marked by filled and open circles, respectively.

nm. The integrated band areas of the acid chloride C═O stretches are used to determine the concentrations of precursor molecules during the experiments. Upon condensation, the integrated IR band areas are less affected by changes in spectral band shape and shifts in the band centers than are simple peak height determinations. To determine the number of UV photons absorbed during photoexcitation, we use standard molar absorptivities obtained directly from our UV spectra. We use integrated gas-phase IR molar absorptivities to calculate the reaction quantum yields.

Results

Figures 2−4 display the infrared spectra of matrix-isolated (argon: 300 to 1) acetyl chloride, propionyl chloride, and valeryl chloride. Each molecule is readily identified by characteristic C═O stretch bands centered at 1808, 1803, and 1807 cm^{-1}, respectively. By comparing spectra of pre- and post-irradiated samples, the consumption of acid chlorides is observed by the distinct decrease in the C═O stretching absorption features. HCl·ketene product complexes form following photoexcitation at 248 and 266 nm. Formation of photoproducts is observed by the emergence of IR bands that correspond to the vibrational modes of HCl·ketene, HCl·methylketene, and HCl·propylketene complexes. These complexes are identified by the HCl and C═O stretch bands at 2685 and 2145 cm^{-1} (Figure 2), 2596−2622 and 2127 cm^{-1} (Figure 3), and 2685 and 2122−2143 cm^{-1} (Figure 4), respectively.

A Beer's law relationship is used to calculate the number of photons absorbed during irradiation. We measure the UV molar absorptivities for acetyl, propionyl, and valeryl chloride at 248 nm to be 32.1 ± 0.2, 37.3 ± 0.2, and 44.0 ± 0.2 L mol^{-1} cm^{-1}, and at 266 nm to be 14.2 ± 0.3, 15.9 ± 0.3, and 20.7 ± 0.3 L mol^{-1} cm^{-1}, respectively. The $\pi^* \leftarrow$ n electronic absorption feature, centered near 240 nm, is relatively unperturbed by the matrix, which allows us to use gas-phase molar absorptivities to calculate the precursor photoabsorption probability.

Gas-phase integrated molar absorptivities for the C═O stretch bands of acetyl chloride [(1.09 ± 0.01) × 10^4 L mol^{-1} cm^{-2}], propionyl chloride [(1.07 ± 0.01) × 10^4 L mol^{-1} cm^{-2}], and valeryl chloride [(0.88 ± 0.01) × 10^4 L mol^{-1} cm^{-2}] are used in calculating acid chloride concentrations. The gas-phase molar absorptivities are identical (within error) to the integrated molar absorptivities of neat thin film acid chloride samples. We choose the C═O stretch band intensity to determine the fraction of photoreacted precursor molecules because this band is only weakly perturbed by the surrounding environment.

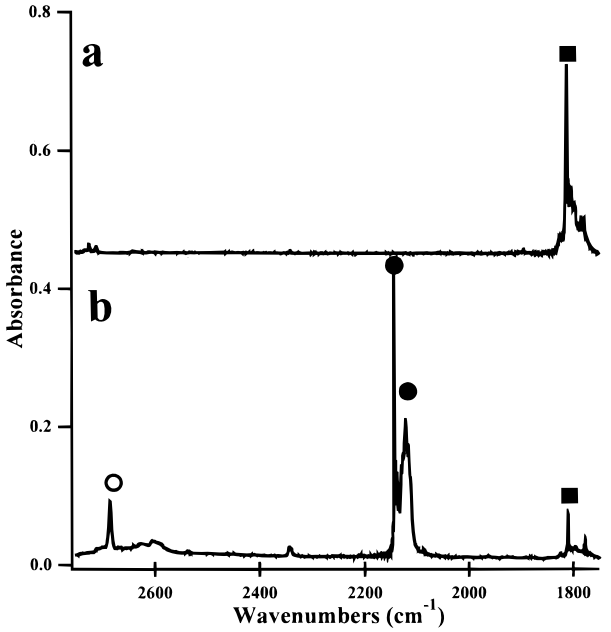

Figure 4. Infrared spectra of valeryl chloride ($CH_3CH_2CH_2CH_2COCl$) before (a) and after (b) 248 nm irradiation. The C═O stretch band of the valeryl chloride is marked by filled squares. The C═O and HCl stretches of the propylketene and HCl are marked by filled and open circles, respectively.

Photoreaction quantum yields for neat and argon matrix-isolated samples irradiated at 248 and 266 nm are reported in Table 1. The yields for argon matrix-isolated samples irradiated

TABLE 1: Reaction Quantum Yields for Neat and Argon Matrix-Isolated Acid Chlorides Irradiated at 248 and 266 nm[a]

	248 nm		266 nm	
	neat	Ar matrix	neat	Ar matrix
CH_3COCl	0.21 ± 0.05	0.36 ± 0.06	0.20 ± 0.05	0.44 ± 0.04
CH_3CH_2COCl	0.07 ± 0.04	0.20 ± 0.04	0.12 ± 0.04	0.20 ± 0.04
$CH_3(CH_2)_3COCl$	0.13 ± 0.04	0.15 ± 0.05	0.10 ± 0.04	0.18 ± 0.05

[a] Error bars represent combined statistical and estimated systematic errors.

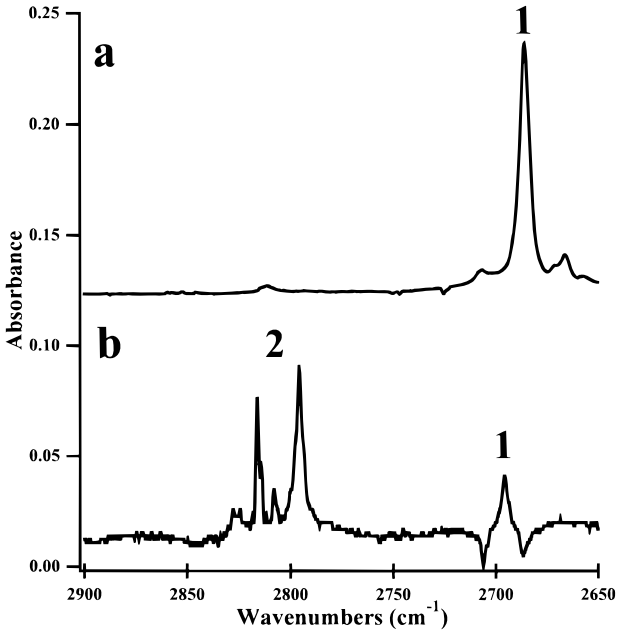

Figure 5. Infrared difference spectra of the HCl region in HCl·ketene complexes following 248 nm irradiation of acetyl chloride in argon (a) and in xenon (b) matrixes. The HCl band centers assigned to structures **1** and **2** are marked.

at 248 nm closely agree with the quantum yields for 266 nm irradiation. However, the quantum yields of matrix-isolated samples are approximately twice those of the condensed neat samples. The acetyl chloride quantum yield (0.44 ± 0.04) is greater than that of propionyl (0.20 ± 0.04) and valeryl (0.18 ± 0.05) chlorides. The quantum yield for matrix-isolated propionyl chloride (in argon) is within the experimental error of the valeryl chloride quantum yield, even though valeryl chloride has 18 additional vibrational modes.

HCl Spectra. For argon matrix-isolated acetyl chloride irradiated at 248 nm, the IR band of the HCl·ketene dimer is centered at 2686 cm^{-1} with an estimated integrated molar absorptivity of 1.0×10^4 L mol^{-1} cm^{-2} (Figure 5a). This absorption band has previously been assigned to the HCl stretch of structure **1**.[2] Other experimental evidence to confirm the assignment of the dimer geometry is the center frequency of the ketene C═O stretch band at 2142 cm^{-1} (Figure 6a) that is identical to that of argon matrix-isolated noncomplexed ketene.[23] Thus, we would expect the C═O center frequency to be shifted if structure **2** were formed. The lack of frequency shift of the C═O stretch band is attributed to the lack of hydrogen bonding to the ketene oxygen (structure **1**).

We find distinct differences between HCl·ketene spectra in argon versus xenon matrixes. Spectral differences between the argon and xenon samples are due, in part, to different intermolecular bonding in HCl·ketene complexes that we will show to correspond to structures **1** and **2**. In a xenon matrix, HCl IR bands are observed at 2696 and 2798 cm^{-1}. Similarly, two

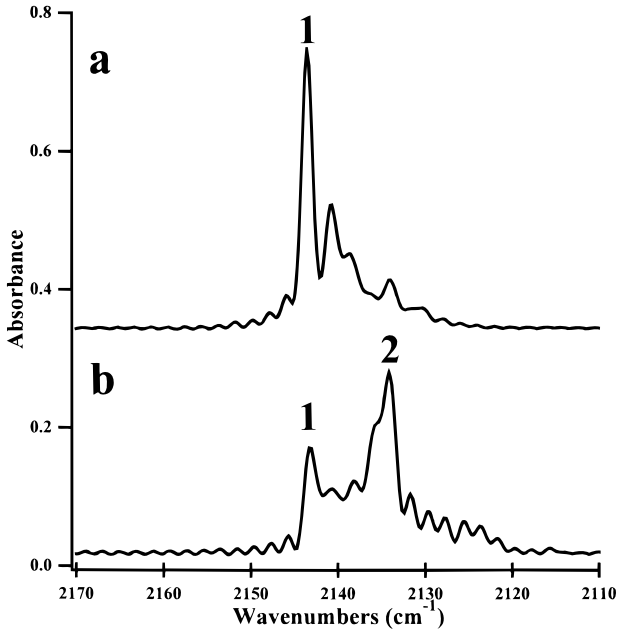

Figure 6. Infrared difference spectra of the ketene C═O stretch region in argon (a) and xenon matrixes (b). The C═O stretches assigned to structures **1** and **2** are marked.

TABLE 2: Experimental and Calculated Band Shifts of the C═O Ketene Stretch and HCl IR Band Centers for Structures 1 and 2[a]

structure, band	$\Delta\nu$ (exp) (cm^{-1})	$\Delta\nu$ (theor) (cm^{-1})
1, C═O stretch	0	2
2, C═O stretch	9	8
1, HCl	202	206
2, HCl	55	50

[a] Experimental band shifts are determined by comparison of matrix-isolated monomer and complex center frequencies. Calculated shifts are obtained from ref 19 and are determined from free monomer and complex center frequencies.

ketene C═O stretch bands are observed at 2142 and 2134 cm^{-1}. The HCl and C═O stretch bands at 2696 and 2142 cm^{-1} are assigned to structure **1**, as observed in argon matrixes. The HCl and C═O stretch bands at 2798 and 2134 cm^{-1} are attributed to structure **2**, as observed in xenon matrixes. A molar absorptivity of 0.6×10^4 L mol^{-1} cm^{-2} is measured for the 2798 cm^{-1} HCl band of structure **2**, which is less than the molar absorptivity for the 2686 cm^{-1} band of structure **1**. Experimental and calculated frequency shifts for structures **1** and **2** are given in Table 2.

Discussion

Matrix environments often shift infrared band centers to frequencies lower than gas-phase values and may significantly increase the integrated IR band intensities.[24] This is especially true in a hydrogen-bonded system such as water, where the O—H stretch band intensity increases by a factor of ~30, on a per molecule basis, for the condensed-phase system.[25] HCl itself displays an IR absorption intensity increase of 5.5 upon condensation.[26] Therefore, extreme care must be employed when using H-atom stretch band intensities for quantitative yield determinations in condensed-phase systems. One must account for the significant variations in band intensities that may occur between systems with relatively minor structural differences. Fortunately, much smaller frequency and integrated intensity shifts are observed for carbonyl stretch bands, as the surrounding

molecules do not significantly perturb the C═O functional group absorption dipole. The integrated C═O absorption strength is nearly identical for gas- and condensed-phase systems such that far less error is introduced by band intensity variations. Similarly, matrix effects do not appear to significantly perturb the electronic $\pi^* \leftarrow$ n transition, as gas- and condensed-phase UV spectra both display peak absorption near 240 nm and bandwidths of roughly 40 nm (fwhm).

We obtain nearly identical reaction quantum yields following 248 and 266 nm excitation. Similar quantum yields are expected because absorption at 248 and 266 nm excites the same $\pi^* \leftarrow$ n electronic transition. While small changes in the photexcitation energy (5.00 versus 4.66 eV) do not alter the reaction quantum yield, the yields are significantly reduced for neat thin film samples when compared to the argon matrix-isolated samples. For the β-substituted molecules, CH_3CH_2COCl and $CH_3CH_2CH_2CH_2COCl$, we obtain quantum yields that are both roughly half that of CH_3COCl.

These results can be rationalized by considering the flow of the initial photoexcitation energy into the reaction coordinate, the intramolecular vibrations, or the surrounding matrix. The relative disposition of the initial excitation determines the reaction yield. Following photoexcitation of the C═O ($\pi^* \leftarrow$ n) transition, the C═O bond stretches due to the occupation of the π^* state. Upon $S_1 \rightarrow S_0$ interconversion, the initial energy is localized along the C═O bond. The localized energy may then lead to elongation of the C—Cl bond and distortion of the C—C═O and C—C—Cl angles along the reaction coordinate. This scenario couples energy in a mode specific way directly into the reaction coordinate, leading to rapid reaction. If, however, sufficient intramolecular energy transfer occurs prior to reaction, then vibrational relaxation may result instead of reaction. Alternatively, the surrounding matrix may quench the initial photoexcitation, where quenching efficiency will likely be different for argon, xenon, and neat matrixes.

The reaction quantum yields are similar for CH_3CH_2COCl and $CH_3CH_2CH_2CH_2COCl$; molecules possessing 24 and 42 vibrational modes, respectively. Therefore, the internal energy following $S_1 \rightarrow S_0$ interconversion must not distribute statistically into the vibrational modes of the acid chlorides. If this were the case, the quantum yields would drastically decrease with the increase in the number of vibrational modes. Since the reaction quantum yield is similar for CH_3CH_2COCl and $CH_3CH_2CH_2CH_2COCl$, the photoreaction cannot be described by a statistical reaction rate theory (RRKM).

We find that the product quantum yields are affected by the presence of an alkyl chain, as the yield for CH_3COCl is twice that of CH_3CH_2COCl or $CH_3CH_2CH_2CH_2COCl$. The alkyl chain not only increases the number of vibrational modes but also reduces, from three to two, the number of α-H-atoms available for the elimination reaction. Furthermore, alkyl substitution introduces isomeric and geometric considerations, similar to steric hindrance, into the reaction. The steric hindrance induced by alkyl groups is analogous to the steric effects reported for the photochemistry of matrix-isolated chloroformylketene (ClOCCH═C═O).[27] Chloroformylketene (acetylketene) is produced in cis and trans conformations following a direct elimination reaction from malonyl dichloride ($ClOCCH_2COCl$). The cis conformer of matrix-isolated acetylketene is properly aligned such that HCl and carbon suboxide (O═C═C═C═O) are formed following photolysis at wavelengths greater than 310 nm (excitation associated with the ketene portion of acetylketene). Photolysis of *trans*-acetylketene will not produce the HCl and C_3O_2 products because chlorine is hindered from interacting with the α-H-atom. Similarly, alkyl groups of acid chlorides can place H-atoms at positions that are less favorable to reaction.

Energy relaxation will be more efficient in neat matrixes than argon or xenon matrixes. In neat matrixes, surrounding acid chloride molecules have a greater number of resonant vibrational modes that are more able to receive energy due to better energy matching. This is consistent with observed gas-phase collision energy transfer results that show increased energy transfer rates for greater numbers of vibrational modes and for better energy matching of vibrational modes.[15]

HCl·Ketene Structure. The effects of hydrogen bonding on vibrational modes have been experimentally and theoretically studied[24,28] and show a general trend that correlates hydrogen-bond strength to shifts in infrared frequencies and band intensities. Generally, the greater the hydrogen-bond strength, the greater the red shift of IR band centers, the greater the integrated IR intensity, the greater molecular bond length, and the lesser the hydrogen-bond length. These trends have been observed in the ab initio electronic structure study of the complexes displayed in Figure 1.[19]

We previously assigned the HCl·ketene complex formed in argon matrixes to structure **1** on the basis of polarization data and the calculated transition-state structure of the acetyl chloride unimolecular reaction that forms HCl·ketene.[2] However, we did not have actual dimer calculations to further confirm the assignment. We now revisit that assignment in light of current experimental data and new calculations.[19] As seen in Table 2, the 206 cm^{-1} red shift from calculated frequencies of free to complexed HCl agrees well with our measured red shift of 202 cm^{-1}. Furthermore, no hydrogen bonding occurs on the oxygen of structure **1**, which results in no change between the matrix-isolated and observed dimer frequencies at 2142 cm^{-1}.[23] A similar structure was assigned to the dimer of HCl·O═C═C═C═O produced by the >310 nm photolysis of *cis*-chloroformylketene (Cl—CO—CH═C═O).[29] This assignment was made by comparing the experimental red shift of the HCl IR band to calculated frequency shifts.

The assignment of structure **2** to the HCl·ketene complex found in xenon matrixes is based on comparing experimental red shifts of the HCl and ketene C═O stretches to calculated values. The HCl IR bands are red shifted by 55 cm^{-1} from the xenon matrix-isolated HCl frequencies in good agreement with the calculated value of 50 cm^{-1} from the free to complexed HCl frequencies (Table 2).[19] The decrease in the magnitude of observed and calculated IR red shifts, for HCl·H_2C═C═O structures **1** and **2**, is similar to that calculated for HCl·O═C═C═C═O complexes.[29] The C═O stretch frequency is useful for assigning structure **2** because it can be used to probe the position of the hydrogen bond along the ketene molecule. In structure **2**, the oxygen of ketene is involved in a hydrogen bond, which results in red shifting the C═O stretch band. An experimental red shift of 9 cm^{-1} is observed, which closely agrees with the calculated red shift of 8 cm^{-1}. Furthermore, the magnitude of the IR frequency shifts, binding energies, and integrated molar absorptivities agree with the general trends predicted for hydrogen-bonding complexes.

Both structures **1** and **2** are formed in xenon matrixes following 248 and 266 nm photoexcitation of acetyl chloride. Structure **1** represents the global minimum[31] with a binding energy of 1.37 kcal mol^{-1}, and structure **2** corresponds to the local minimum with a binding energy of 0.71 kcal mol^{-1}.[19] It is interesting that most of the complexes in xenon matrixes are the less stable structure **2**. It is possible that the differences in

lattice spacing are responsible for the preponderance of structure **2**. Argon matrixes have a unit cell spacing of ~5.4 Å with a nearest neighbor distance of ~3.8 Å compared to xenon, which has a unit cell spacing of ~6.2 Å with a nearest neighbor distance of ~4.4 Å.[30] The photoreaction of acetyl chloride in argon has less volume available for the photoproducts. Photoreactions in xenon matrixes have more space for molecular rearrangement such that other HCl·ketene structures and little polarization dependence are expected. This is experimentally observed for both 248 and 266 nm photoreactions in xenon matrixes. The larger spacing of the xenon matrixes does not appear to alter the quantum yields much, as values determined in both matrixes are similar.

Conclusions

Photoexcitation of acetyl, propionyl, and valeryl chlorides at 248 and 266 produces HCl·ketene, HCl·methylketene, and HCl·propylketene complexes. The initial photoexcited state undergoes interconversion $S_1 \rightarrow S_0$, leading to local excitation of the carbonyl group and then distortion of the α-C−C and C−Cl bonds. This scenario allows for direct motion along the reaction coordinate to the transition state, without statistical energy distribution into the acid chloride vibrational modes. We report reaction quantum yields, which display a dependence upon the molecular structure and matrix composition. Lengthening the alkyl chain lowers quantum yields by reducing the number of α-H-atoms available for the elimination reaction and through steric hindrance of acid chloride alkyl groups. We measure quantum yields in neat matrixes to be roughly half that in argon or xenon matrixes. We attribute this difference to greater relaxation rates (quenching) in the neat matrix, perhaps due to the greater number of vibrational modes.

We assign structures for HCl and ketene complexes in argon and xenon matrixes by comparing IR spectra to ab initio results. In argon matrixes, the product complex HCl frequency is strongly shifted (202 cm^{-1}) whereas the ketene remains unshifted with respect to matrix-isolated ketene, indicating structure **1**. In xenon matrixes, HCl·ketene complexes display an absorption band indicative of both structures **1** and **2** following 248 and 266 nm irradiation of acetyl chloride. The complexed HCl frequency of **2** is less shifted (55 cm^{-1}) than for **1** but the C═O band of the complexed ketene now displays a 9 cm^{-1}, shift which corresponds to HCl hydrogen-bonded to the ketene oxygen. Differences between HCl·ketene structures in argon and xenon matrixes are attributed to the size of the matrix cage. The argon matrix has a smaller lattice spacing that is more restrictive to intermolecular rearrangement than in the xenon matrix.

Acknowledgment. The authors were supported by the Divisions of Chemical Sciences of the Office of Basic Energy Sciences, U.S. Department of Energy. Pacific Northwest National Laboratory is operated for the U.S. Department of Energy by Battelle under contract No. DE-AC06-76RLO 1830. We also acknowledge Chris Fuller for assistance in obtaining data.

References and Notes

(1) Rowland, B.; Hess, W. P. *Chem. Phys. Lett.* **1996**, *263*, 574.
(2) Rowland, B.; Hess, W. P. *J. Phys. Chem. A* **1997**, *101*, 8049.
(3) Deshmukh, S.; Hess, W. P. *J. Chem. Phys.* **1994**, *100*, 6429.
(4) Deshmukh, S.; Myers, J. D.; Xantheas, S. S.; Hess, W. P. *J. Phys. Chem.* **1994**, *98*, 12535.
(5) Shibata, T.; Suzuki, T. *Chem. Phys. Lett.* **1996**, *262*, 115.
(6) Lane, I. C.; Meehan, R.; Powis, I. *J. Phys. Chem.* **1995**, *99*, 12371.
(7) Sumathi, R.; Chandra, A. K. *J. Chem. Phys.* **1993**, *99*, 6531.
(8) Martin, X.; Moreno, M.; Lluch, J. M. *J. Phys. Chem.* **1993**, *97*, 12186.
(9) Winter, P. R.; Rowland, B.; Hess, W. P.; Radziszewski, J. G.; Nimios, M. R.; Ellison, G. B. *J. Phys. Chem. A* **1998**, *102*, 3238.
(10) Steinfeld, J. I.; Francisco, J. S.; Hase, W. L. *Chemical Kinetics and Dynamic*, 1st ed.; Prentice Hall Inc.: Englewood Cliffs, NJ, 1989.
(11) Tsang, W. *J. Chem. Phys.* **1964**, *41*, 2487.
(12) Laursen, S. L.; Pimentel, G. C. *J. Phys. Chem.* **1990**, *94*, 8175.
(13) Srivatsava, A.; Arunan, E.; Manke, G.; Setser, D. W.; Sumathi, R. *J. Phys Chem. A* **1998** 102, 6412.
(14) Pearson, M. *Kinetics and Mechanism*, 3rd ed.; John Wiley & Sons: New York, 1981.
(15) Miller, L. A.; Barker, J. R. *J. Chem. Phys.* **1996**, *105*, 1383.
(16) Blass, P. M.; Jackson, R. C.; Polanyi, J. C.; Weiss, H. *J. Chem. Phys.* **1991**, *94*, 7003.
(17) Berg, O.; Ewing, G. E. *J. Phys. Chem.* **1991**, *95*, 2908.
(18) Sumathi, R.; Chandra, A. K. *Chem. Phys.* **1994**, *181*, 73.
(19) Sumathi, R.; Chandra, A. K. *Chem. Phys. Lett.* **1997**, *271*, 287.
(20) Groner, P.; Stolkin, I.; Gunthard, H. H. *J. Phys. E* **1973**, *6*, 122.
(21) *Aldrich: Catalog Handbook of Fine Chemicals*; Aldrich Chemical Co.: Milwaukee, WI, 1996.
(22) Sinnock, A. C. *J. Phys. C.* **1980**, *13*, 2375.
(23) Moore, C. B.; Pimentel, G. C. *J. Phys. Chem.* **1963**, *38*, 2816.
(24) Pimentel, G. C.; McClellan, A. L. *The Hydrogen Bond*; Freeman: San Fracisco, 1960.
(25) Whalley, E.; Klug, D. D. *J. Chem. Phys.* **1986**, *84*, 4807.
(26) Chesnoy, J.; Ricard, D.; Flytzanis, C. *Chem. Phys.* **1979**, *42*, 337.
(27) Pietri, N.; Chiavassa, T.; Allouche, A.; Rajzmann, M.; Aycard, J. *J. Phys. Chem.* **1996**, *100*, 7034.
(28) Ojamae, L.; Hermansson, K. *J. Phys. Chem.* **1994**, *89*, 4271.
(29) Pietri, N.; Chiavassa, T.; Allouche, A.; Aycard, J. P. *J. Phys. Chem. A* **1997**, *101*, 1093.
(30) Raff, L. M. *J. Chem. Phys.* **1990**, *93*, 3160.
(31) We note that the accuracy of these calculations is insufficient to unambiguously assign relative energies that differ by only 0.6 kcal mol^{-1}. In fact, our own electronic structure calculations, for the HCl·methylketene complex, indicates that the most stable structure involves bonding at the oxygen site.